Acta Materialia 207 (2021) 116703

Contents lists available at ScienceDirect

Acta Materialia

journal homepage: www.elsevier.com/locate/actamat

A combinatorial approach to study the phase constitution of the Ni-Al-Pt system

G.H. Cao[a,*], Z. Zhang[a], X. Li[a,b,*], W. Skrotzki[c], E. Müller[d], R. Schneider[d], D. Gerthsen[d]

[a] State Key Laboratory of Advanced Special Steel & School of Materials Science and Engineering, Shanghai University, 99 Shangda Road, Shanghai 200444, China
[b] School of Materials Science and Engineering, Shanghai Jiao Tong University, Shanghai 200240, China
[c] Institute of Solid State and Materials Physics, Technische Universität Dresden, Dresden D-01062, Germany
[d] Laboratory for Electron Microscopy, Karlsruhe Institute of Technology (KIT), Karlsruhe D-76128, Germany

ARTICLE INFO

Article history:
Received 6 October 2020
Revised 5 January 2021
Accepted 25 January 2021
Available online 28 January 2021

Keywords:
Ni-Al-Pt
Diffusion
Microstructure
Phase transformation
Transmission electron microscopy (TEM)

ABSTRACT

Platinum has a beneficial effect on improving alumina scale adhesion and decreasing the alpha alumina growth of aluminide bond coats in thermal barrier coatings. However, complex phases form among Ni, Al and Pt during service due to diffusion between bond coat and underlying Ni-base superalloy substrate. A combinatorial/high-throughput approach to study alloy phase equilibria with precious compositions is high-efficient and cost-saving. The microstructural evolution of a Ni-Al-Pt diffusion triple fabricated by annealing at 1100°C for 96 h followed by water-cooling was characterized by transmission electron microscopy and electron probe microanalysis. The high temperature Pt_3Al(h) phase is stabilized due to dissolved Ni, indicating that Ni is a stabilizer for Pt_3Al(h). A ternary phase, Ni_2PtAl, predicted to exist, has been observed experimentally with $L1_2$ structure adjacent to $(Ni,Pt)_3Al$, while the $L1_0$-structured tetragonal $NiPt_2Al$ phase is also confirmed in the Ni-Al-Pt system. Upon cooling, the Ni-rich β-(Ni,Pt)Al undergoes a martensitic transformation from β (B2) to β'-(Ni,Pt)Al ($L1_0$). The orthorhombic D^{19}_{2h}-structured $(Ni,Pt)_5Al_3$ phase with lattice parameters $a = 0.747$ nm, $b = 0.682$ nm, and $c = 0.376$ nm was found to form from β'-(Ni,Pt)Al martensite. The orientation relationship of D^{19}_{2h} and β' phases is (100)[010] D^{19}_{2h} // (100)[001] β'. (221) twins are observed in lamellar $(Ni,Pt)_5Al_3$. Phase constitution is determined in the Ni-Al-Pt system at 1100°C. The mechanism of formation of $(Ni,Pt)_5Al_3$ from β'-(Ni,Pt)Al was analyzed.

1. Introduction

Nickel-base superalloys are utilized in aircraft and widely in power-generation turbine engines because of an excellent combination of elevated-temperature strength, toughness, and resistance to degradation in oxidizing or hot-corrosive environments [1–3]. Cuboidal γ'-Ni_3Al precipitates with coherent interfaces with the γ-Ni(Al) matrix and cube-on-cube crystallographic orientation relationship form the classic two-phase $\gamma + \gamma'$ microstructure. The $L1_2$ structured γ' precipitate is the primary strengthening phase and key prerequisite for the success of nickel-base superalloys. Any further significant improvements in efficiency of an engine require much higher operating temperatures, particularly for the components in advanced gas-turbine engines. However, superalloys are already used at up to 90% of their melting temperatures [4]. Therefore, advanced cooling schemes coupled with thermal barrier coatings (TBCs) are extremely important and enable the current superalloy components to meet much more severe operating conditions. TBCs afford a temperature reduction of approximately 140°C, thereby preventing thermomechanical failure of the components [5]. State-of-the-art TBCs consist of a three-layered architecture. The top coat is a ceramic thermal insulator, the intermediate thermally grown oxide (TGO) layer provides oxidation resistance, and the metallic bond coat (BC) adheres to the substrate and aids in the formation of the TGO. The typical BC is made of nickel aluminides, which is designed to supply enough aluminium to enable the formation of α-Al_2O_3 in preference to other oxides. During thermal cycling the interdiffusion between BC and the underlying Ni-base superalloy matrix at high-temperature results in the formation of Al-rich to Ni-rich phases [6,7]. Upon cooling the Ni-rich β-NiAl phase will undergo a martensitic transformation from β (B2) to β'-NiAl ($L1_0$) [8–15]. During continuous growth of the TGO layer the concentration of Al is further reduced causing the

* Corresponding authors.
E-mail addresses: ghcao@shu.edu.cn (G.H. Cao), lx_net@sina.com (X. Li).

https://doi.org/10.1016/j.actamat.2021.116703
1359-6454/

phase transformation from β to γ' in BC [6,16]. It is known that Pt is a beneficial addition for improving the high temperature oxidation resistance as well as the adhesion of the TGO to BC [3,17–19]. It has been shown that Pt addition prevents the formation of brittle Ni-rich oxides in Ni-Al alloys with low Al content [20]. However, the effect of Pt is still not well understood, because there is a paucity of information pertaining to the phase equilibria in the Ni-Al-Pt system.

Experimental works [19,21–30] and first-principles calculations [31–35] have attempted to shed light on the complicated Ni-Al-Pt system. For example, Jackson and Rairden [21] studied the Ni-Al-Pt isothermal section by analyzing the chemistry and morphology of the oxidation of platinum-aluminide coatings on Inconel 738 alloy at 1060°C, and did not find any Ni-Al-Pt ternary phases. In contrast, a ternary $NiPt_2Al$ phase was observed in the phase stability study of $(Ni,Pt)_3Al$ alloys at 1100°C by Kamm and Milligan [22]. The compositional range of the $NiPt_2Al$ phase was determined. At fixed Al composition of 25 at.%, the single-phase $L1_0$ structured $NiPt_2Al$ field exists at least from 37 to 50 at.% Pt. Later, the same ternary $NiPt_2Al$ phase was reported by Meininger and Ellner [23] in the annealed $Ni_{0.75-x}Pt_xAl_{0.25}$ ($0.37 \leq x_{Pt} \leq 0.50$) alloys at 1000°C, while a continuous solid solution between the Ni_3Al and Pt_3Al phases was not found. Recently, Gleeson et al. [19,24] studied the partial Ni-Al-Pt phase diagrams at 1100°C and 1150°C by solid-solid diffusion couples. The most noteworthy finding is a ternary phase, denoted as α-NiPt(Al), which possesses a $L1_0$-type structure. It has a large Pt solubility ranging from about 33 - 66 at.% and skews along an almost constant Pt/Al ratio of 1.5. Based on diffraction of synchrotron radiation the unit cell of α-NiPt(Al) is the same as that of $NiPt_2Al$, which is consistent with that reported by Grushko et al. [27,28]. Jiang et al. [31,32], Lu et al. [33], Alam et al. [34], and Liu et al. [35] have studied the phase stability in Ni-Al-Pt with a combination of first-principles calculations, a cluster expansion technique and a Monte Carlo simulation, yielding two ordered structures, Ni_2PtAl and $NiPt_2Al$, the latter being in good agreement with experiments [22–30]. In addition, Grushko et al. [27,28] found out that at 1100°C the Pt_2Al_3, Pt_2Al, and Pt_3Al phases dissolve up to 4, 5, and 15 at.% Ni, respectively, but their crystal structures with Ni solution have not been analyzed. At higher Al content (33.5 ~ 37.3 at.%), in the Ni-Al system an orthorhombic D^{19}_{2h} structured Ni_5Al_3 phase, first identified by Enami and Nenno [36], can form. The Ni_5Al_3 phase displays a martensite-like morphology and is believed to form via β' martensite or β-NiAl [36–40]. Because of many unknown aspects and inconsistent results especially with Pt solution, the Ni_5Al_3 phase still appears to be a relatively peculiar phase.

A combinatorial approach offers a unique opportunity to characterize the phase stability and interdiffusion characteristics of a wide variety of multicomponent systems. Moreover, the use of diffusion multiples to study alloy phase equilibria especially with precious metals could be highly efficient and cost-saving [25,41]. It is the aim of this research to get a deeper and more comprehensive understanding of the effect of Ni on the stability of Pt-Al compounds, to explore the phase constitution of ternary phases including Ni_2PtAl and $NiPt_2Al$, and to understand the formation mechanism of the $(Ni,Pt)_5Al_3$ phase. For this purpose, a solid-liquid-solid Ni/Al/Pt diffusion triple was prepared without any clamps, and the assembly is pressed into a nickel tube and sealed with nickel caps by electron beam welding in vacuum. Pure Al as one component can supply enough Al to form the Al-rich phases in the interdiffusion zones. Details are shown in Fig. 1 of the experimental section and in our previous work [42]. The phase constitution after annealing at 1100°C was analyzed by using scanning electron microscopy (SEM), electron probe microanalysis (EPMA), transmission electron microscopy (TEM), and high-angle annular dark-field scanning transmission electron microscopy (HAADF-STEM) combined with energy dispersive X-ray spectroscopy (EDXS).

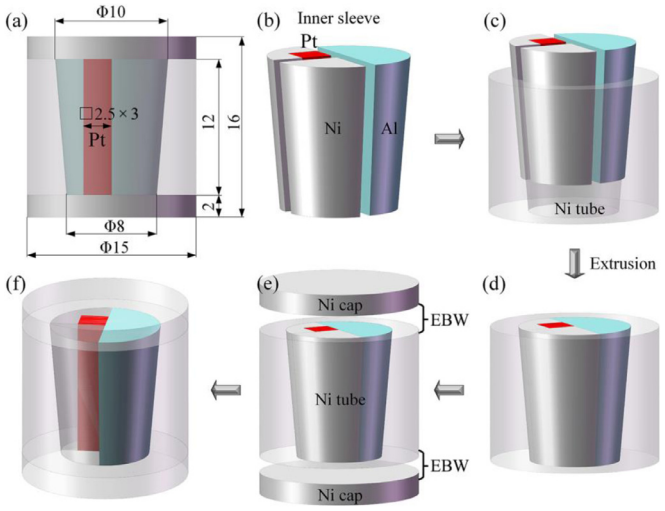

Fig. 1. Schematic illustration of the Ni/Al/Pt diffusion triple: (a) longitudinal section dimensions (in mm), (b) inner structure, and (c–f) assembly using extrusion and electron-beam welding (EBW).

2. Experimental procedure

The Ni-Al-Pt diffusion triple was manufactured by Al, Ni, and Pt of 4N purity. As shown in Fig. 1a, all parts of the diffusion triple were cut into shapes by electrical discharge machining (EDM), ground to 5000-grit finish using SiC papers, and ultrasonically cleaned in acetone. The Pt block was arranged in the inner sleeve (consisting of Al and Ni blocks), as shown in Fig. 1b. The inner sleeve and the Ni tube were assembled as displayed in Fig. 1c and d. Next, two Ni caps were placed on the ends of the Ni tube (Fig. 1e) and electron-beam welded (EBW, SEBW60-6P) in vacuum of 1×10^{-2} Pa (Fig. 1f). This design can prevent Al from evaporation or oxidation and isolate any interstitial contaminants that may diffuse into the inner sleeve during the annealing process. The Ni/Al/Pt diffusion triple was then sealed in a high-purity quartz tube under an argon atmosphere and annealed at (1100 ±1)°C for 96 h in a muffle furnace (LAC LH15/13). In order to preserve the high-temperature state, cooling was established by breaking the quartz tube in water. The diffusion triple was cut in half parallel to the caps by EDM, ground and polished without etching.

Operated at an acceleration voltage of 20 kV a Shimadzu 1720 EPMA coupled with wavelength dispersive X-ray spectroscopy (WDS) was used to measure the composition profiles of the interdiffusion zone at an accuracy of ~3 at.%. Before the preparation of TEM specimens, surface micrographs of the interdiffusion zone were taken by SEM in LEO Gemini 1530 and FEI Helios 600i microscopes. Focused-ion-beam (FIB, FEI Strata 400 and 600i) milling was used to prepare cross-section TEM lamellae with the standard lift-out technique [43]. TEM bright-field (BF) imaging and selected area electron diffraction (SAED) were performed in JEOL 2010F, Philips CM 200 and FEI Tecnai G2 electron microscopes equipped with field emission guns operated at an acceleration voltage of 200 kV. The distribution of Al, Ni, and Pt was analyzed by HAADF-STEM in combination with EDXS using JEOL 2100F and FEI Tecnai Osiris transmission electron microscopes operated at an acceleration voltage of 200 kV.

3. Results

Fig. 2a is a cross-sectional backscattered-electron (BSE) SEM micrograph showing a representative interdiffusion zone of a Ni/Al/Pt diffusion triple after 96 h annealing at 1100°C, followed by wa-

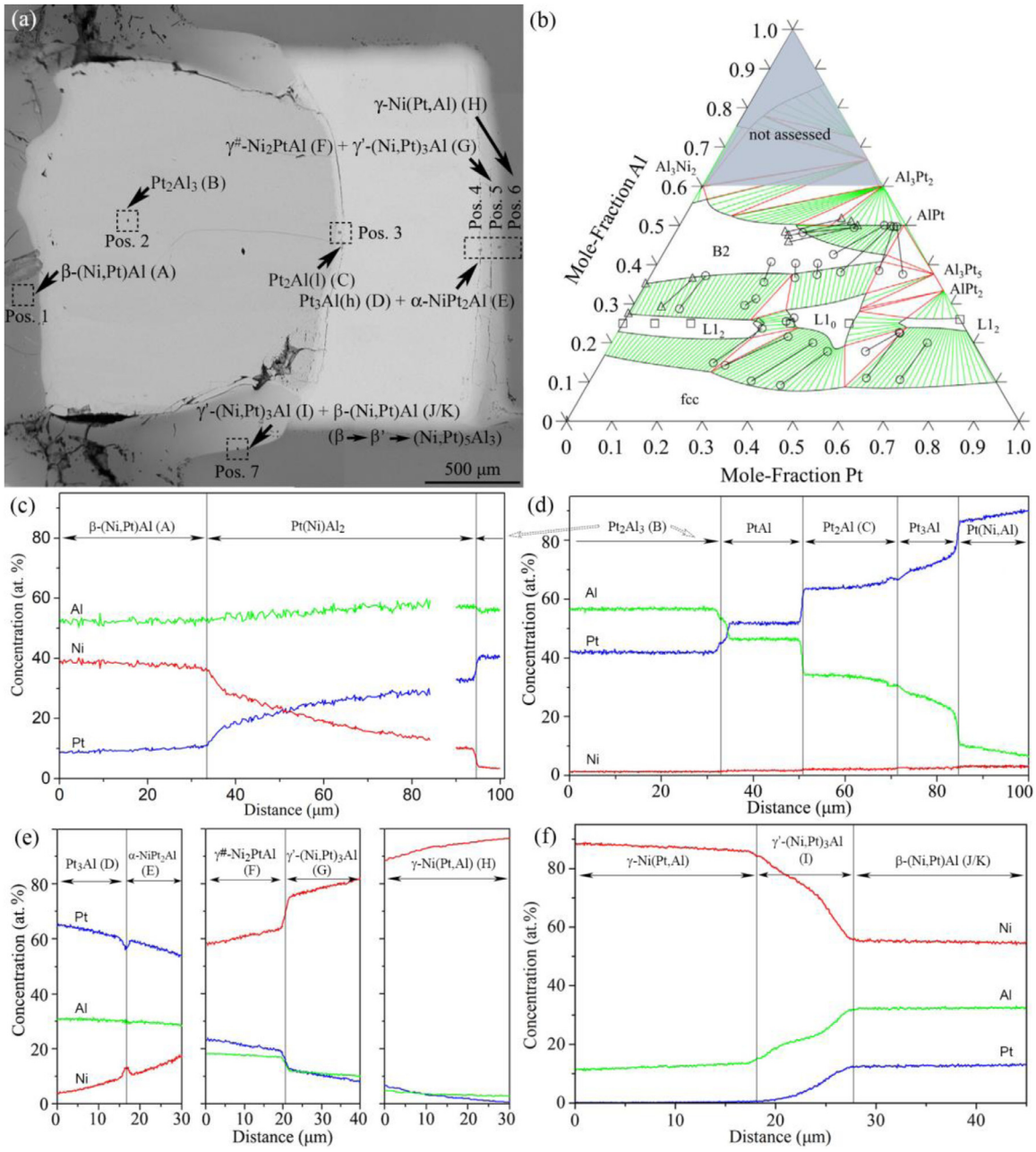

Fig. 2. (a) Cross-sectional BSE SEM micrograph of Ni/Al/Pt diffusion triple. Positions (Pos.) 1 - 7 are places where TEM specimens were prepared by FIB milling, (b) the isothermal section of Ni-Al-Pt at 1100°C [35], EPMA concentration profiles of the Pos. (c) 1, (d) 2 and 3, (e) 4 - 6, and (f) 7. The capital letters behind the phase assignments are markers for regions studied by TEM.

ter cooling. Fig. 2b shows the isothermal section of Ni-Al-Pt at 1100°C determined by Liu et al. [35], and fcc, $L1_2$, $L1_0$ and B2 represent γ-Ni(Pt,Al), γ'-$(Ni,Pt)_3Al$ (left) /Pt_3Al (right), α-$NiPt_2Al$ and β-(Ni,Pt)Al, respectively. The EPMA concentration line profile of position (Pos.) 1 shown in Fig. 2c indicates that this area may belong to the Al-rich β-(Ni,Pt)Al phase. Pos. 2 also analyzed by EPMA reveals the presence of Al and Pt with an approximate Pt to Al ratio of 2: 3 with 0.5 - 2.0 at.% Ni and therefore corresponds to the Pt_2Al_3 phase (Fig. 2d) [44]. The area between Pos. 1 (β-(Ni,Pt)Al) and Pos. 2 (Pt_2Al_3) could be $Pt(Ni)Al_2$ based on the EPMA concentration profiles shown in Fig. 2c. The EPMA concentration profiles in Fig. 2d at Pos. 3 also contain 1.7 - 3.0 at.% Ni, with a Pt: Al ratio close to 2: 1, revealing the Pt_2Al phase, and PtAl, Pt_3Al and Pt(Ni,Al) phases exist as shown in Fig. 2d. Fig. 2e shows EPMA concentration profiles across the Pos. 4 - 6 indicating that the multilayered interdiffusion zones are possibly comprised of Pt_3Al, α-$NiPt_2Al$, $\gamma^{\#}$-Ni_2PtAl, γ'-$(Ni,Pt)_3Al$, and γ-Ni(Pt,Al). According to the EPMA concentration profiles shown in Fig. 2f, Pos. 7 may consist of γ'-$(Ni,Pt)_3Al$ and Ni-rich β-(Ni,Pt)Al, the occurrence of β'-(Ni,Pt)Al martensite in Pos. 7 in the following TEM investigation (Fig. 9) further demonstrates that such martensite forms due to martensitic transformation of Ni-rich β-(Ni,Pt)Al during water cooling. The left side of the γ'-$(Ni,Pt)_3Al$ phase in Fig. 2f is γ-Ni(Pt,Al). The detailed phase assignments will be precisely made by considering TEM SAED patterns.

Fig. 3a is a TEM BF image of the FIB lamella taken at Pos. 1 in Fig. 2a. Fig. 3b–d are the SAED patterns of the region marked as A in Fig. 3a along the [102], [001], and [113] zone axes, respectively. Indexing indicates that Pos. 1 has a typical ordered body-centered cubic (bcc) B2 structure with lattice parameter $a = 0.289$

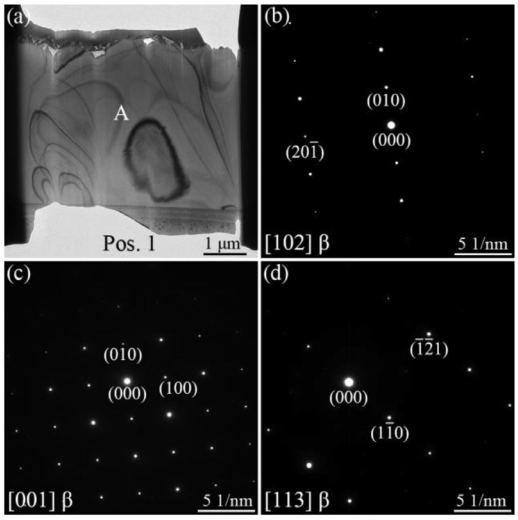

Fig. 3. (a) TEM BF image from Pos. 1, SAED patterns of the region marked as A (β-(Ni,Pt)Al) along the (b) [102], (c) [001], and (d) [113] zone axes.

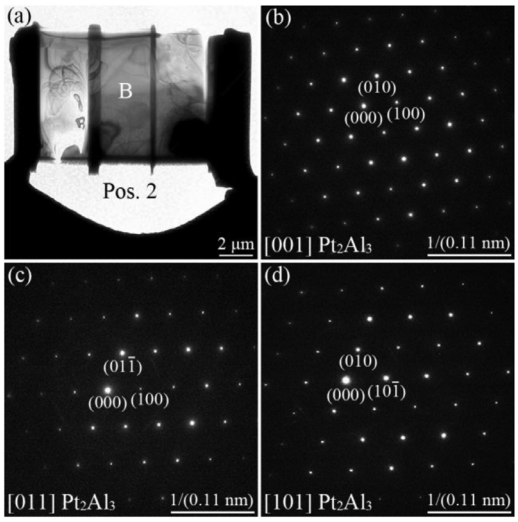

Fig. 4. (a) TEM BF image from Pos. 2, SAED patterns of the region marked as B (Pt_2Al_3) along the (b) [001], (c) [011], and (d) [101] zone axes.

nm. Therefore, this region is the β-(Ni,Pt)Al phase in combination with the EPMA measurement shown in Fig. 2c.

Fig. 4a is a TEM BF image of the FIB lamella from Pos. 2 in Fig. 2a. Fig. 4b–d are the SAED patterns of the region marked as B in Fig. 4a along the [001], [011], and [101] zone axes, revealing a hexagonal structure with lattice parameters $a = 0.423$ nm and $c = 0.516$ nm. Thus, based on EPMA composition analysis we conclude that Pt_2Al_3 [44] phase is present at Pos. 2.

Pos. 3 in Fig. 5a exhibits a globular morphology. Fig. 5b–d are the SAED patterns of the region C along the [100], [201], and [103] zone axes. Indexing shows that it is an orthorhombic Pt_2Ga-type structure with lattice parameters $a = 1.683$ nm, $b = 0.395$ nm, and $c = 0.540$ nm. On the basis of the EPMA measurements Pos. 3 is deduced to be low-temperature Pt_2Al [44] phase with 1.7 - 3.0 at.% Ni.

EPMA concentration profiles of the Pos. 4 in Fig. 2e (D and E) indicate that the Al content is slightly decreased, while the Ni content increases with decrease of Pt. Pos. 4 shows two kinds of morphologies in the TEM BF image of Fig. 6a, one is a lath structure marked as D and the other is globular structure marked as E. As shown in an enlarged TEM image in Fig. 6b, the region D consists

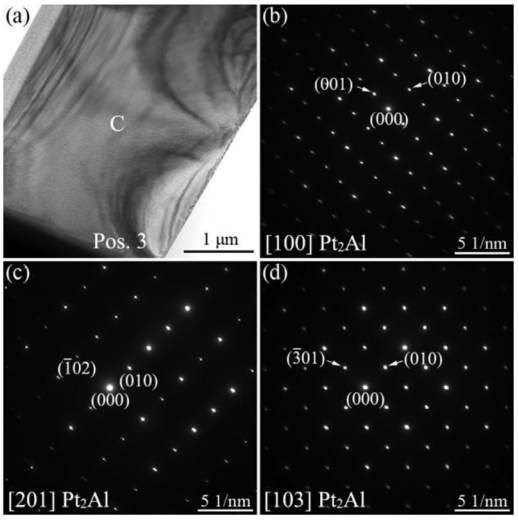

Fig. 5. (a) TEM BF image from Pos. 3, SAED patterns of the region C (Pt_2Al) along the (b) [100], (c) [201], and (d) [103] zone axes.

of fine bands or platelets. Fig. 6c–e are the SAED patterns of one band along the [100], [101], and [103] zone axes. In combination with the EPMA results presented in Fig. 2e, it is concluded that the region D is high-temperature face-centered cubic $L1_2$-structured Pt_3Al [44] with lattice parameter $a = 0.382$ nm containing ~3.6 - 10 at.% Ni. Fig. 6f–h are the SAED patterns of the region E along the [001], [110], and [112] zone axes. Indexing indicates that region E is a face-centered tetragonal (fct) $L1_0$ structure with lattice parameters $a = 0.390$ nm, and $c = 0.361$ nm [24]. The Pt content in this region is about 54 - 60 at.%, and the Ni: Pt: Al ratio is close to 1: 2: 1. Hence, the region E should be the ternary $NiPt_2Al$ phase, i.e. α-NiPt(Al).

Fig. 7a is a TEM BF image from Pos. 5 in Fig. 2a showing an interface between regions F and G. Fig. 7b–d are the SAED patterns of the region F along the [001], [013], and [011] zone axes revealing that it has a $L1_2$ structure with lattice parameter $a = 0.368$ nm. The Ni: Pt: Al ratio of region F is about 2: 1: 1, indicating the Ni_2PtAl phase [31], denoted as $\gamma^{\#}$. Fig. 7e is the SAED pattern of the region G along the [011] zone axis. Thus, it belongs to $L1_2$-structured γ'-$(Ni,Pt)_3Al$ with lattice parameter $a = 0.359$ nm. Fig. 7f is the superposition of the SAED patterns of $\gamma^{\#}$-Ni_2PtAl (F) and γ'-$(Ni,Pt)_3Al$ (G) showing the orientation relationship of $(\bar{1}\bar{3}1)[013]$ $\gamma^{\#}$//$(3\bar{1}1)[011]$ γ', which is equivalent to $\{100\}<001>\gamma^{\#}$//$\{100\}<001>\gamma'$. Fig. 8a is a TEM BF image of the FIB lamella from Pos. 6 in Fig. 2a and SAED patterns of the region H shown in Fig. 8b and c indicating that Pos. 6 is fcc γ-Ni(Pt,Al) with lattice parameter $a = 0.351$ nm.

Fig. 9a is the TEM BF image from Pos. 7 in Fig. 2a showing the globular and lamellar morphologies. Fig. 9b–d are the SAED patterns of the region marked as I along the [001], $[\bar{1}11]$ and [011] zone axes. Region I is γ'-$(Ni,Pt)_3Al$, which is similar to the region G in Fig. 7a. Fig. 9e is a HAADF-STEM image of the frame in upper right area in Fig. 9a, and the corresponding EDXS mappings of Ni, Al and Pt revealing their homogeneous distributions. The SAED patterns from plate J along different zone axes are shown in Fig. 9f–h. Indexing indicates that the plate has an orthorhombic Pt_5Ga_3-type D^{19}_{2h} structure [36] with lattice parameters $a = 0.747$ nm, $b = 0.682$ nm, and $c = 0.376$ nm. Therefore, the plate J is $(Ni,Pt)_5Al_3$.The presence of reflection streaking in Fig. 9g is due to the lamellar microstructure of the plate. Fig. 9i is a high-magnification TEM BF image of plate J displaying finer platelets inside. The platelets are twin-related and the twin plane is (221). Fig. 9j–l are the SAED patterns of plate K corresponding to [010]

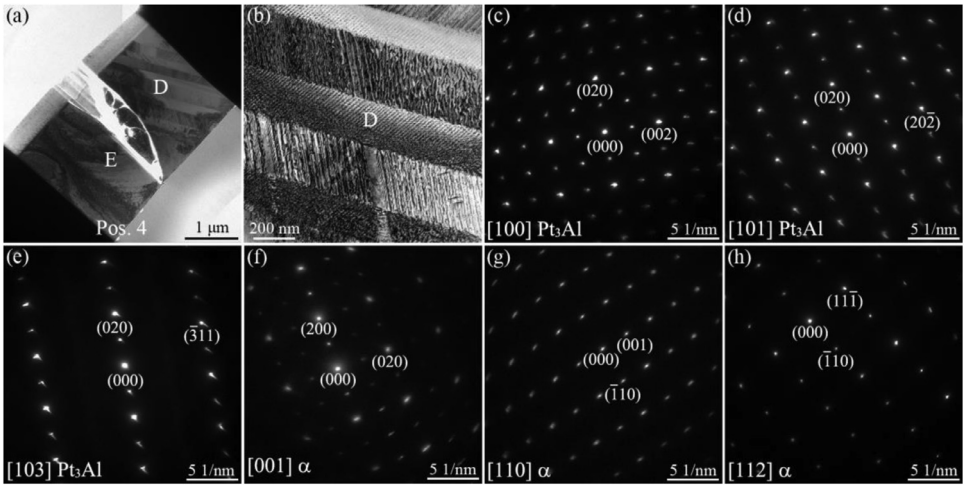

Fig. 6. (a) TEM BF image from Pos. 4, (b) an enlarged TEM BF image of the region D showing a lamellar morphology, SAED patterns of the region D (Pt_3Al) along the (c) [100], (d) [101], and (e) [103] zone axes, and the globular region E (α-$NiPt_2Al$) along the (f) [001], (g) [110], and (h) [112] zone axes. The bright regions in (a) are vacuum regions due to cracks in the FIB-prepared TEM specimen.

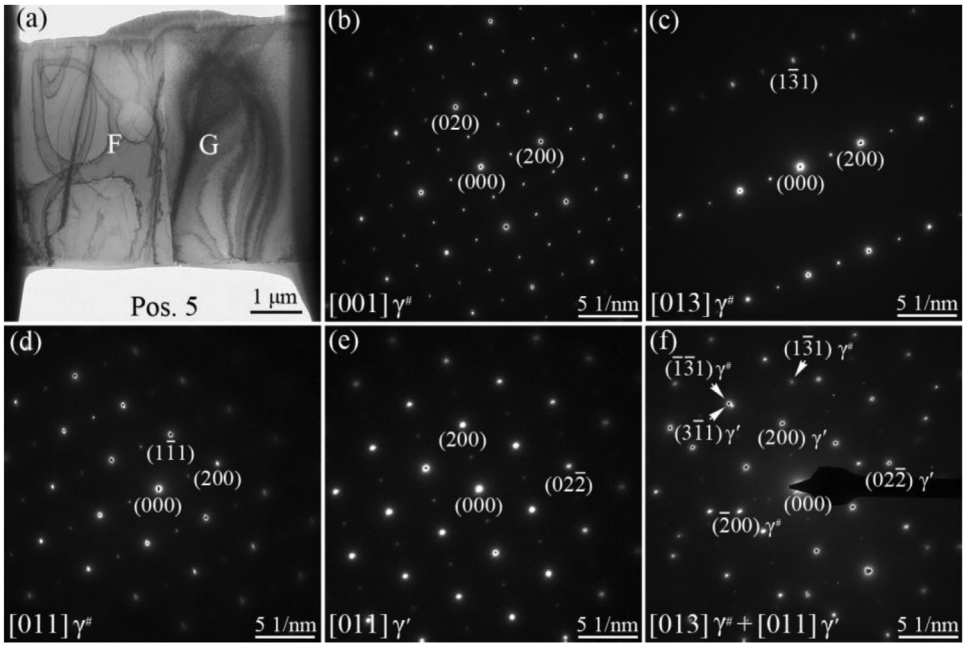

Fig. 7. (a) TEM BF image from Pos. 5 showing an interface between the regions F and G, SAED patterns of the region F ($\gamma^{\#}$-Ni_2PtAl) along the (b) [001], (c) [013], and (d) [011] zone axes, SAED pattern of the region G (γ'-$(Ni,Pt)_3Al$) along the (e) [011] zone axis, and (f) the composite SAED patterns of $\gamma^{\#}$ and γ' phases showing the orientation relationship $(\bar{1}\bar{3}1)[013]\ \gamma^{\#}$ // $(3\bar{1}1)[011]\ \gamma'$.

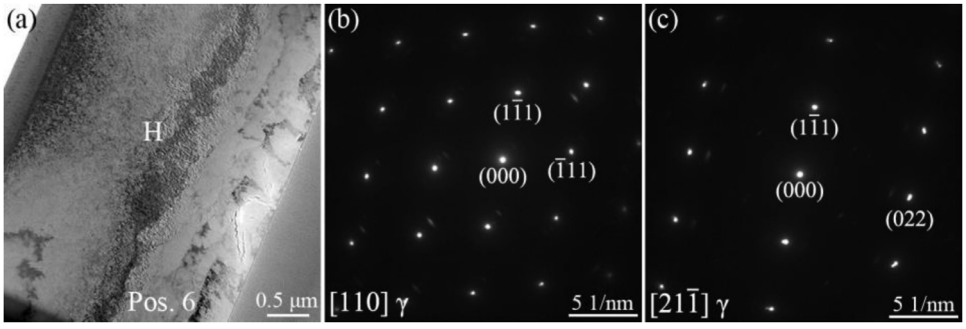

Fig. 8. (a) TEM BF image from Pos. 6, and SAED patterns of the region marked as H (γ-Ni(Pt,Al)) along the (b) [110] and (c) $[21\bar{1}]$ zone axes.

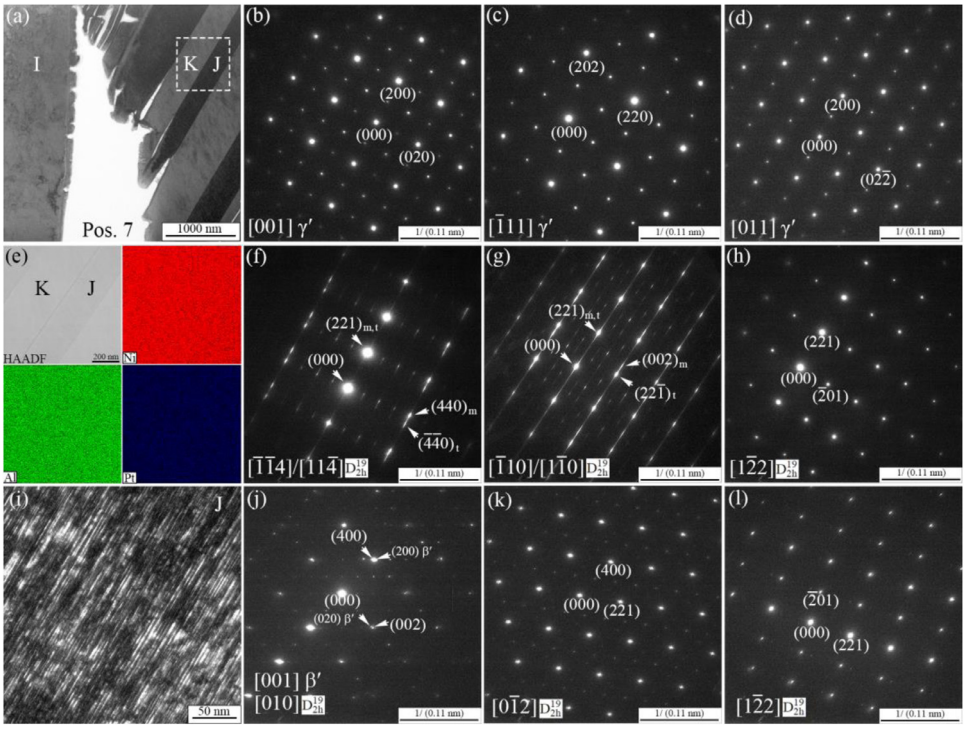

Fig. 9. (a) TEM BF image from Pos. 7 showing globular and lamellar regions, SAED patterns of the region marked as I (γ') along the (b) [001], (c) [$\bar{1}$11], and (d) [011] zone axes, (e) HAADF-STEM image of the region in the frame in Fig. 9a and the corresponding EDXS mappings of Ni, Al and Pt, SAED patterns of the region J along the (f) [11$\bar{4}$], (g) [1$\bar{1}$0], and (h) [1$\bar{2}$2] zone axes, (i) high-magnification of the region J ($(Ni,Pt)_5Al_3$) showing (221) twin boundaries, SAED patterns of the region K ($(Ni,Pt)_5Al_3$) along the (j) [010], (k) [0$\bar{1}$2], and (l) [1$\bar{2}$2] zone axes. The bright regions in (a) are vacuum regions due to cracks in the FIB-prepared TEM specimen.

(Fig. 9j), [0$\bar{1}$2] (Fig. 9k), and [1$\bar{2}$2] (Fig. 9l) zone axes, respectively. The SAED pattern in Fig. 9l is the same as that of Fig. 9h, indicating that the plate K is also $(Ni,Pt)_5Al_3$. The other set of reflections in Fig. 9j corresponds $L1_0$ β'-(Ni,Pt)Al (a = 0.381 nm, c = 0.325 nm) martensite along the [001] zone axis. The observation of β' martensite is a strong indication that this area is Ni-rich β-(Ni,Pt)Al before cooling, in accord with the EPMA concentration profiles shown in Fig. 2f. The composite SAED patterns of the D^{19}_{2h} $(Ni,Pt)_5Al_3$ and $L1_0$ β'-(Ni,Pt)Al in Fig. 9j show an orientation relationship of (100)[010] D^{19}_{2h} // (100)[001] β'.

4. Discussion

The phase constitution of the Ni-Al-Pt system was efficiently determined by the combinatorial approach without preparation of bulk Ni-Al-Pt alloys with different compositions. Compositional and microstructural analysis of the interdiffusion zones of the Ni/Al/Pt diffusion triple indicate that the Pt_2Al_3, Pt_2Al, Pt_3Al, β-(Ni,Pt)Al, β'-(Ni,Pt)Al, γ-Ni(Pt,Al), γ'-$(Ni,Pt)_3Al$, $\gamma^{\#}$-Ni_2PtAl, α-$NiPt_2Al$, and $(Ni,Pt)_5Al_3$ phases exist as summarized in Table 1. It has been found that the stability of the Pt_3Al phase is affected by some amounts of Ni. A ternary $L1_2$ $\gamma^{\#}$-Ni_2PtAl phase predicted by first-principle calculations is observed beside the $L1_0$ α-$NiPt_2Al$ phase. The phase transformation of β to β'-(Ni,Pt)Al and $(Ni,Pt)_5Al_3$ is further elucidated.

4.1. Stability of Pt_2Al and Pt_3Al phases

The binary Pt-Al phase diagram is complicated and the nominal phases Pt_3Al, Pt_2Al, Pt_5Al_3, PtAl, Pt_2Al_3, $PtAl_2$, Pt_8Al_{21}, and Pt_5Al_{21} can develop. Among them, Pt_2Al and Pt_3Al are isotypic [44]. The high-temperature Pt_2Al(h) phase shows a Ni_2Si-type structure and has a solubility range of 1 to 2 at.%, at ~1060°C. Pt_2Al(h) will transform to the low-temperature Pt_2Al(l) with the Pt_2Ga(l)-type structure and a solubility range of 1 to 2 at.%. Similarly, Pt_3Al(h) with Cu_3Au-type $L1_2$ structure and a solubility range of about 10 at.% below 1290°C transforms into Pt_3Al(l) with Pt_3Ga(l)-type DO_c' structure, with a solubility range of 4 at.% at 859°C [45–48]. EPMA compositional analyses show that Pt_2Al and Pt_3Al phases are composed of ~ 1.7 - 3.0 and 3.6 - 10 at.% Ni, respectively. SAED patterns shown in Fig. 6 indicate that the solubility of Ni in Pt_3Al is in favor of the formation of the high-temperature Pt_3Al(h) phase, revealing that Ni is a stabilizer for Pt_3Al(h).

The important factor of a third element on the structural stability of Pt_3Al is the atomic radius. An element with a smaller atomic radius that substitutes Pt (0.139 nm) should favor the fcc $L1_2$ structure. Ni (0.125 nm) or Cr (0.128 nm) atoms, which are smaller than Pt, will occupy the Pt sites and stabilize the $L1_2$ form of Pt_3Al(h) [49–53]. The minority element leads to a higher electron concentration and favors the tetragonal DO_c' structure. Gohle and Schubert [54] reported that the addition of Si resulted in the $Pt_3Al_{1-x}Si_x$ ($x \leq 10$ at.%) phase with DO_c' structure at low-temperature, dis-

Table 1
Phases determined in Ni-Al-Pt diffusion triple.

Position	Phase	Type	Lattice parameters (nm) a	b	c
Pos. 1	β-(Ni,Pt)Al	CsCl	0.289		
Pos. 2	Pt_2Al_3	Ni_2Al_3	0.423		0.516
Pos. 3	Pt_2Al(l)	Pt_2Ga(l)	1.683	0.395	0.540
Pos. 4	Pt_3Al(h)	Cu_3Au	0.382		
	α-NiPt(Al) ($NiPt_2Al$)	CuAu	0.390		0.361
Pos. 5	$\gamma^{\#}$-Ni_2PtAl	Cu_3Au	0.368		
	γ'-$(Ni,Pt)_3Al$	Cu_3Au	0.359		
Pos. 6	γ-Ni(Pt,Al)	Cu	0.351		
Pos. 7	γ'-$(Ni,Pt)_3Al$	Cu_3Au	0.359		
	β'-(Ni,Pt)Al	CuAu	0.381		0.325
	$(Ni,Pt)_5Al_3$	Pt_5Ga_3	0.747	0.682	0.376

playing that Si is a Pt_3Al(l) stabilizer. Si is also known as a α-Ti stabilizer element [55]. So far, one cannot be certain to what extent the low-temperature Pt_2Al(l) phase observed is induced by solid solution of Ni or thermodynamically driven since Pt_2Al(l) could have formed from Pt_2Al(h) on cooling, as the transformation temperature in the binary system is at about 1060°C.

4.2. Microstructural evolution from Ni_3Al to Pt_3Al

In the γ'-Ni_3Al phase the Ni atoms exclusively occupy the face centers and the Al atoms the cube corners. Previous studies [31–35] revealed that Pt has a strong preference for the Ni site in Ni_3Al. With the increasing Pt content during diffusion, the Pt atoms will occupy the Ni sites on the {100} face centers in the γ' phase and form the $L1_2$-structured $\gamma^{\#}$-Ni_2PtAl in Pos. 5F as confirmed by SAED patterns (Fig. 7b–d) and EPMA measurements (Fig. 2e). The orientation relationship of $\{100\}\langle001\rangle\gamma^{\#}//\{100\}\langle001\rangle\gamma'$ reveals a small lattice mismatch (~2.5%) between the $\gamma^{\#}$ and γ' phases inducing low internal stress. When the Pt content increases up to 50 at.%, the Pt and Ni atoms occupy the prismatic (100) and (010) face centers and the (001) face center of the basal plane, respectively, resulting in α-$NiPt_2Al$ phase formation as observed in the diffusion region in Pos. 4E and confirmed by SAED patterns (Fig. 6f–h). As the Pt content keeps further increasing, the Pt_3Al phase (Pos. 4D, Fig. 6c–e) will form.

4.3. Formation of $(Ni,Pt)_5Al_3$

In the Ni-Al binary system, the Ni-rich β-NiAl (62 - 69 at.%) usually undergoes a diffusionless martensitic transformation on cooling. The resultant martensite has $L1_0$ structure with either *ABC* (3*R*) stacking or *ABCABAC* (7*R*) stacking depending on the alloy composition, and is {111} internally twinned. Both martensitic transformations in β-(Ni,Pt)Al bond coatings and bulk alloys have been observed [9–12,15,16,38,56–59]. As we know, M_s (martensitic transformation start temperature) is very sensitive to the alloy composition. A change in Ni composition by as little as 1 at.% changes M_s by as much as 100°C [60]. A high Pt content increases the temperature range where upon cooling the parent B2 β-(Ni,Pt)Al transforms to fct $L1_0$ β'-(Ni,Pt)Al martensite. For instance, M_s for Ni-39Al-15Pt and Ni-37Al-30Pt (at.%) alloys was reported to be about 861°C and 1100°C, respectively [9,61]. According to the compositions measured by EPMA in Fig. 2f and SAED patterns in Fig. 9 showing that the β'-(Ni,Pt)Al martensite coexists with $(Ni,Pt)_5Al_3$, it is deduced that M_s could be higher than ~700°C, a temperature, where the Ni_5Al_3 phase forms based on the Ni-Al phase diagram [6].

The Ni_5Al_3 phase could disturb the shape memory effect of the Ni-Al system in the Ni-rich part and, therefore, is also a matter of interest [62]. TEM investigations indicate that the lattice parameters of D_{2h}^{19} Ni_5Al_3 approximately are: $a = 2b_0$, $b = 2c_0$, and $c = a_0$, with a_0, b_0, and c_0 lattice parameters of β'-NiAl martensite ($a_0 = b_0$). Therefore, the D_{2h}^{19} structure has a unit cell volume four times that of $L1_0$ β'-NiAl [36]. SAED patterns reveal that the orientation relationship between the D_{2h}^{19} and $L1_0$ phases is (100)[010] D_{2h}^{19} // (100)[001] β', which further demonstrate the accuracy of the crystal structure constitution of D_{2h}^{19} Ni_5Al_3 shown in Figs. 3–5 in Ref. 36. This orientation relationship means that the lattice of D_{2h}^{19} in [010] direction is superimposed on the lattice of the $L1_0$ phase in [001] direction. The lattice mismatch along these directions is $\delta = (d_{(010)}D_{2h}^{19} - 2d_{(001)}\beta')/2d_{(001)}\beta' \approx 2.8\%$, indicating low internal stress between the D_{2h}^{19} and $L1_0$ phases.

The TEM results shown in Fig. 9 suggest that the formation of $(Ni,Pt)_5Al_3$ may undergo two stages. Firstly, the martensitic transformation from Ni-rich β-(Ni,Pt)Al to β'-(Ni,Pt)Al is taking place with Bain orientation relationship, involving a Bain distortion of the *c/a* ratio of 0.707 (B2) to 0.85 ($L1_0$). No atomic diffusion and re-ordering is required in this step. Secondly, as excess Ni atoms migrate and substitute Al on the Al sublattice, then shuffle or reorder, $(Ni,Pt)_5Al_3$ is formed. The *c/a* ratio of $(Ni,Pt)_5Al_3$ is about 0.89. Therefore, the $(Ni,Pt)_5Al_3$ phase is more closely related to the $L1_0$ martensite from the point of view of tetragonal configuration and atomic arrangement [36,38,63,64]. Since Pt increases the diffusion in NiAl, the $(Ni,Pt)_5Al_3$ phase already forms upon cooling, whereas the formation of Ni_5Al_3 phase is extremely sluggish and can take days, weeks, or even years [65,66].

5. Conclusions

The Ni/Al/Pt diffusion triple has been proved to be a successful approach with high efficiency for studying the phase constitution with precious metals. Based on the EPMA and TEM investigations, the following main conclusions can be drawn:

(1) Ni appears to be a stabilizer for the high temperature Pt_3Al (h). Pt_2Al (l) is identified as an orthorhombic structure with lattice parameters a = 1.683 nm, b = 0.395 nm, and c = 0.540 nm. Pt_3Al (h) exhibits a cubic $L1_2$ structure with lattice parameter a = 0.382 nm.

(2) A ternary cubic phase, $\gamma^{\#}$-Ni_2PtAl, predicted by ab initio simulations was observed with lattice parameter a = 0.368 nm. It is located adjacent to γ'-$(Ni,Pt)_3Al$ and has an orientation relationship (100)[001] $\gamma^{\#}$ // (100)[001] γ'. The $L1_0$ α-$NiPt_2Al$ ternary phase is also confirmed.

(3) The D_{2h}^{19} structured $(Ni,Pt)_5Al_3$ phase forms from $L1_0$ β'-(Ni,Pt)Al martensite and shows an orthorhombic crystal structure with lattice parameters a = 0.747 nm, b = 0.682 nm, and c = 0.376 nm. (221) twin boundaries exist between the $(Ni,Pt)_5Al_3$ plates. The D_{2h}^{19} $(Ni,Pt)_5Al_3$ phase has an orientation relationship (100)[010] D_{2h}^{19} // (100)[001] β' with the $L1_0$ β'-(Ni,Pt)Al martensite.

Declaration of Competing Interest

The authors declare that they have no known competing financial interests or personal relationships that could have appeared to influence the work reported in this paper.

Acknowledgment

This work was supported by the Shanghai Committee of Science and Technology, China, under grant number 16520721700, the National Natural Science Foundation of China (NSFC) under grant numbers 51271107 and 51690164, the Network for Functional Nanostructures funded by the Baden-Württemberg Foundation and the Alexander von Humboldt Foundation for a renewed research stay. G.H. Cao would like to thank Dr. P.F. Hu and J.C. Peng of Shanghai University, and A.Q. Xu of Southeast University for part of the TEM investigations.

References

[1] C.T. Sims, N.S. Stoloff, W.C. Hagel, in: Superalloys II: High-Temperature Materials for Aerospace and Industrial Power, Wiley, New York, 1987, pp. 27–57.
[2] T.M. Pollock, S. Tin, Nickel-based superalloys for advanced turbine engines: chemistry, microstructure and properties, J. Propul. Power 22 (2006) 361–374.
[3] B. Gleeson, Thermal barrier coatings for aeroengine applications, J. Propul. Power 22 (2006) 375–383.
[4] R.E. Schafrik, R. Sprague, Saga of gas turbine materials: part II, Adv. Mater. Process. 162 (2004) 27–30.
[5] M. Peters, C. Leyens, U. Schulz, W.A. Kaysser, EB-PVD thermal barrier coatings for aeroengines and gas turbines, Adv. Eng. Mater. 3 (2001) 193–204.
[6] D.R. Clarke, C.G. Levi, Materials design for the next generation thermal barrier coatings, Annu. Rev. Mater. Res. 33 (2003) 383–417.

[7] S. Darzens, D.R. Mumm, D.R. Clarke, A.G. Evans, Observations and analysis of the influence of phase transformations on the instability of the thermally grown oxide in a thermal barrier system, Metall. Mater. Trans. A 34 (2003) 511–522.

[8] P. Boullay, D. Schryvers, J.M. Ball, Nano-structures at martensite macrotwin interfaces in $Ni_{65}Al_{35}$, Acta Mater. 51 (2003) 1421–1436.

[9] D.J. Sordelet, M.F. Besser, R.T. Ott, B.J. Zimmerman, W.D. Porter, B. Gleeson, Isothermal nature of martensite formation in Pt-modified β-NiAl alloys, Acta Mater. 55 (2007) 2433–2441.

[10] M.W. Chen, M.L. Glynn, R.T. Ott, T.C. Hufnagel, K.J. Hemker, Characterization and modeling of a martensitic transformation in a platinum modified diffusion aluminide bond coat for thermal barrier coatings, Acta Mater. 51 (2003) 4279–4294.

[11] M.W. Chen, R.T. Ott, T.C. Hufnagel, P.K. Wright, K.J. Hemker, Microstructural evolution of platinum modified nickel aluminide bond coat during thermal cycling, Surf. Coat. Technol. 163-164 (2003) 25–30.

[12] S. Rosen, J.A. Goebel, The crystal structure of nickel-rich NiAl and martensitic NiAl, Trans. Met. Soc. AIME 242 (1968) 722–724.

[13] J.L. Smialek, Martensite in NiAl oxidation-resistant coatings, Metall. Trans. 2 (1971) 913–915.

[14] E.G. Lesnikova, V.P. Lesnikov, Influence of instability of the β-phase of the aluminide coating on the condition and scale resistance of the surface layer of Ni-Al alloys, Met. Sci. Heat Treat. 28 (1986) 372–376.

[15] Y. Zhang, J.A. Haynes, B.A. Pint, I.G. Wright, W.Y. Lee, Martensitic transformation in CVD NiAl and (Ni,Pt)Al bond coatings, Surf. Coat. Technol. 163-164 (2003) 19–24.

[16] V.K. Tolpygo, D.R. Clarke, Surface rumpling of a (Ni,Pt)Al bond coat induced by cyclic oxidation, Acta Mater. 48 (2000) 3283–3293.

[17] J.L. Cocking, G.R. Johnston, P.G. Richards, Protecting gas turbine components, Platinum Met. Rev. 29 (1985) 17–26.

[18] I.M. Allam, H.C. Akuezue, D.P. Whittle, Influence of small Pt additions on Al_2O_3 scale adherence, Oxid. Met. 14 (1980) 517–530.

[19] B. Gleeson, W. Wang, S. Hayashi, D.J. Sordelet, Effects of platinum on the interdiffusion and oxidation behavior of Ni-Al-based alloys, Mater. Sci. Forum 461-464 (2004) 213–222.

[20] B.A. Pint, The role of chemical composition on the oxidation performance of aluminide coatings, Surf. Coat. Technol. 188-189 (2004) 71–78.

[21] M.R. Jackson, J.R. Rairden, The aluminization of platinum and platinum-coated IN-738, Metall. Trans. A 8 (1977) 1697–1707.

[22] J.L. Kamm, W.W. Milligan, Phase stability in $(Ni,Pt)_3Al$ alloys, Scr. Metall. Mater. 31 (1994) 1461–1464.

[23] H. Meininger, M. Ellner, Phase transformation and the type of lattice distortion of some platinum-rich phases belonging to the Cu family, J. Alloys Compd. 353 (2003) 207–212.

[24] S. Hayashi, S.I. Ford, D.J. Young, D.J. Sordelet, M.F. Besser, B. Gleeson, α-NiPt(Al) and phase equilibria in the Ni-Al-Pt system at 1150°C, Acta Mater. 53 (2005) 3319–3328.

[25] R.J. Thompson, J.-C. Zhao, K.J. Hemker, Effect of ternary elements on a martensitic transformation in β-NiAl, Intermetallics 18 (2010) 796–802.

[26] W.Y. Gong, L.G. Zhang, H.X. Wei, C.G. Zhou, Phase equilibria, diffusion growth and diffusivities in Ni-Al-Pt system using Pt/β-NiAl diffusion couples, Prog. Nat. Sci. 21 (2011) 221–226.

[27] B. Grushko, D. Kapush, V. Konoval, V. Shemet, A study of the Al-Ni-Pt alloy system. Phase equilibria at 1100 and 1300°C, Powder Metall, Met. Ceram. 50 (2011) 462–470.

[28] B. Grushko, D. Kapush, A refinement of the Al-Ni-Pt phase diagram, J. Alloys Compd. 594 (2014) 127–132.

[29] P. Audigié, A. Rouaix-Vande Put, A. Malié, P. Bilhé, S. Hamadi, D. Monceau, Observation and modeling of α-NiPtAl and Kirkendall void formations during interdiffusion of a Pt coating with a γ-(Ni-13Al) alloy at high temperature, Surf. Coat. Technol. 260 (2014) 9–16.

[30] C.M. Eastman Jr., Vapor-Reacted Diffusion Multiples for Efficient Study of Phase Equilibria and Interdiffusion PhD Thesis, The Ohio State University, 2019.

[31] C. Jiang, D.J. Sordelet, B. Gleeson, First-principles study of phase stability in pseudobinary $(Ni_{1-x}Pt_x)_3Al$ alloys, Phys. Rev. B 72 (2005) 184203.

[32] C. Jiang, M.F. Besser, D.J. Sordelet, B. Gleeson, A combined first-principles and experimental study of the lattice site preference of Pt in B2 NiAl, Acta Mater. 53 (2005) 2101–2109.

[33] X.-G. Lu, B. Sundman, J. Ågren, Thermodynamic assessments of the Ni-Pt and Al-Ni-Pt systems, Calphad 33 (2009) 450–456.

[34] A. Alam, T. Saha-Dasgupta, A. Mookerjee, Ab initio augmented space recursion to study complex multicomponent materials: application to the pseudobinary alloy $Ni_{1-x}Pt_xAl$, Phys. Rev. B 81 (2010) 054201.

[35] X.L. Liu, G. Lindwall, R. Otis, H. Kim, Z.-K. Liu, Thermodynamic remodeling of the Al-Pt system towards an assessment of the Al-Ni-Pt system, Calphad 55 (2016) 88–102.

[36] K. Enami, S. Nenno, A new ordered phase in tempered 63.8Ni-1Co-Al martensite, Trans. Jpn. Inst. Met. 19 (1978) 571–580.

[37] J.H. Yang, C.M. Wayman, On the Ni_5Al_3 phase and related phenomena in a NiAlFe alloy, Mater. Sci. Eng. A 160 (1993) 241–249.

[38] J.H. Yang, C.M. Wayman, On the formation mechanism of Ni_5Al_3 in NiAl-base alloys: part I. Microstructures, Intermetallics 2 (1994) 111–119.

[39] I.M. Robertson, C.M. Wayman, Ni_5Al_3 and the nickel-aluminum binary phase diagram, Metallography 17 (1984) 43–55.

[40] P.S. Khadkikar, K. Vedula, An investigation of the Ni_5Al_3 phase, J. Mater. Res. 2 (1987) 163–167.

[41] J.-C. Zhao, Combinatorial approaches as effective tools in the study of phase diagrams and composition-structure-property relationships, Prog. Mater. Sci. 51 (2006) 557–631.

[42] Z.X. Zhang, H. Jiang, A.M. Russell, W. Skrotzki, E. Müller, R. Schneider, D. Gerthsen, G.H. Cao, Microstructural evolution and phase transformation in the liquid-solid Al/Ni diffusion couple, Philos. Mag. 99 (2019) 1103–1120.

[43] R.M. Langford, C. Clinton, In situ lift-out using a FIB-SEM system, Micron 35 (2004) 607–611.

[44] A.J. McAlister, D.J. Kahan, The Al-Pt (aluminum-platinum) system, Bull. Alloy Phase Diagr. 7 (1986) 47–51.

[45] T. Chattopadhyay, K. Schubert, Crystal structure of $Pt_2Al.r$, J. Less-Common Met. 45 (1976) 79–83.

[46] D. Chatterji, R.C. Devries, J.F. Fleischer, Investigation of sub-solidus equilibria in the platinum-aluminium system using diffusion couples, J. Less-Common Met. 42 (1975) 187–198.

[47] Y. Mishima, Y. Oya, T. Suzuki, $L1_2 \Leftrightarrow D0'_c$ martensitic transformation in Pt_3Al and Pt_3Ga, in: International Conference on Martensitic Transformations, Japan Institute of Metals, Nara, Japan, 1986, pp. 1009–1014.

[48] Y. Oya, Y. Mishima, T. Suzuki, The Pt-Al and Pt-Ga phase diagram with emphasis on the polymorphism of Pt_3Al and Pt_3Ga, Z. Metallkd. 78 (1987) 485–490.

[49] Y. Oya, T. Suzuki, The platinum-germanium phase diagram, Z. Metallkd. 78 (1987) 295–300.

[50] W.D. Callister Jr., Materials Science and Engineering, John Wiley & Sons Ltd, NY, United States, 2003.

[51] R. Völkl, Y. Yamabe-Mitarai, C. Huang, H. Harada, Stabilizing the $L1_2$ structure of $Pt_3Al(r)$ in the Pt-Al-Sc system, Metall. Mater. Trans. A 36 (2005) 2881–2892.

[52] T. Biggs, M.B. Cortie, M.J. Witcomb, L.A. Cornish, Platinum alloys for shape memory applications, Platinum Met. Rev. 47 (2003) 142–156.

[53] P.J. Hill, L.A. Cornish, P. Ellis, M.J. Witcomb, The effects of Ti and Cr additions on the phase equilibria and properties of (Pt)/Pt_3Al alloys, J. Alloys Compd. 322 (2001) 166–175.

[54] R. Gohle, K. Schubert, On the system Platinum- Silicon, Z. Metallkd. 55 (1964) 503–511.

[55] G.H. Cao, G.Y. Jian, N. Liu, W.H. Zhang, A.M. Russell, D. Gerthsen, Microstructure and mechanical properties of an ultrafine Ti-Si-Nb alloy, Mater. Chem. Phys. 163 (2015) 512–517.

[56] K. Enami, S. Nenno, K. Shimizu, Crystal structure and internal twins of the Ni-36.8 at.% Al martensite, Trans. Jpn. Inst. Met. (1973) 161–165.

[57] S. Chakravorty, C.M. Wayman, The thermoelastic martensitic transformation in β' Ni-Al alloys: I. Crystallography and Morphology, Metall. Trans. A 7 (1976) 555–568.

[58] D. Schryvers, Microtwin sequences in thermoelastic Ni_xAl_{100-x} martensite studied by conventional and high-resolution transmission electron microscopy, Philos. Mag. A 68 (1993) 1017–1032.

[59] M. Clancy, M.J. Pomeroy, C. Dickinson, Characterization of 3R martensite in a Ni-40Al-15Pt bulk alloy, J. Alloys Compd. 523 (2012) 11–15.

[60] J.L. Smialek, R.F. Hehemann, Transformation temperatures of martensite in β-phase nickel aluminide, Metall. Trans. 4 (1973) 1571–1575.

[61] G.E. Monastyrsky, P. Ochin, V.V. Odnosum, A.Y. Pasko, V.I. Kolomytsev, Y.N. Koval, Martensitic transformation in Ni-Al-Pt high temperature shape memory alloys, Mater. Sci. Forum 738-739 (2013) 506–514.

[62] D. Schryvers, Y. Ma, The growth of Ni_5Al_3 in $L1_0$ martensite studied by in situ transmission electron microscopy and high resolution electron microscopy, J. Alloys Compd. 221 (1995) 227–234.

[63] D.B. Miracle, Overview No. 104 the physical and mechanical properties of NiAl, Acta Metall. Mater. 41 (1993) 649–684.

[64] J.H. Yang, C.M. Wayman, On the formation mechanism of Ni_5Al_3 in NiAl-base alloys: part II. Kinetics, Intermetallics 2 (1994) 121–126.

[65] K.A. Marino, E.A. Carter, The effect of platinum on defect formation energies in β-NiAl, Acta Mater 56 (2008) 3502–3510.

[66] D. Sengelhoff, U. Koester, On the peritectoid formation of Ni_5Al_3, Intermetallics 5 (1997) 633–640.